BUCKLING AND VIBRATION ANALYSIS OF CIRCULAR HOLLOW SECTION MEMBERS USING GENERALISED BEAM THEORY (GBT)

Cilmar Basaglia

cbasaglia@fec.unicamp.br

School of Civil Engineering Architecture and Urban Design, University of Campinas

Av. Albert Einstein 951, 13083-852, Campinas, Brazil

Dinar Camotim

dcamotim@civil.ist.utl.pt

CEris, ICIST, DECivil, Instituto Superior Técnico, Universidade de Lisboa

Av. Rovisco Pais, 1049-001, Lisboa, Portugal

Nuno Silvestre

nsilvestre@tecnico.ulisboa.pt

LAETA, IDMEC, DEM, Instituto Superior Técnico, Universidade de Lisboa

Av. Rovisco Pais, 1049-001, Lisboa, Portugal

Abstract. *This paper reports the results of an ongoing investigation on the use of Generalised Beam Theory (GBT) to analyse the vibration and buckling behaviours of cold-formed steel circular hollow section (CHS) members. Initially, results concerning the vibration behaviour of load-free steel CHS members are presented and discussed, thus providing a first glimpse of the potential of the GBT-based approach. Then, since it is common practice in literature to express the member static loading as a fraction of its critical buckling value, the buckling behaviour of CHS columns is also addressed. Finally, the vibration behaviour of axially compressed CHS members (columns) is investigated, focusing mainly on the effect of the load magnitude on the fundamental frequency and vibration mode nature. For validation purposes, some GBT results are compared with numerical values obtained from shell finite element analyses carried out in the code ANSYS.*

Keywords: *Vibration analysis, Generalised Beam Theory (GBT), Cold-formed steel members, Circular Hollow Section (CHS) members*

1 INTRODUCTION

Due to the high global and local (wall) slenderness, the structural behaviour and strength of cold-formed steel circular hollow section (CHS) members are invariably governed by local (wall flexure) and/or global (flexural) buckling phenomena (*e.g.*, Teng, 1996). Furthermore, given (i) the well-known mathematical similarity between the stability and vibration analyses (eigenvalue problems), and (ii) the strong influence exerted by local (cross-section) deformation on the buckling behaviour of thin-walled members, it is just logical to expect a comparable effect on the vibration behaviour of such members.

Since most thin-walled steel members are subjected to simultaneous static and dynamic actions, designers are faced with the need of assessing their dynamic response. Therefore, they must be equipped with numerical tools capable of determining the member local and global vibration behaviour, possibly for arbitrary support conditions and in the presence of more or less significant internal forces and/or moments. However, this task can only be rigorously performed at the moment by resorting to shell finite element analysis, a highly computer-intensive approach that requires a substantial modelling effort, including data input and (mostly) result interpretation (*e.g.*, Gardner & Nethercot, 2004).

A very promising alternative to the above approach is the use of a one-dimensional model based on Generalised Beam Theory (GBT), a beam theory incorporating genuine plate theory concepts, *i.e.*, accounting for the member cross-section in- and out-of-plane deformations. In this context, the authors have been employing GBT-based beam finite element formulations to analyse the (i) buckling behaviour of CHS members (*e.g.*, Silvestre, 2007) and (ii) buckling and vibration behaviour of members exhibiting open and/or closed flat-walled cross-sections (*e.g.*, lipped channel and rectangular hollow sections) (*e.g.*, Camotim *et al.*, 2010).

The objective of this work is to present the development, numerical (finite element) implementation of a novel GBT formulation to analyse the vibration and buckling behaviours of thin-walled CHS members, as well as illustrate its application and capabilities. Initially, results concerning the vibration behaviour of load-free steel CHS members are presented and discussed, thus providing a first glimpse of the potential of the GBT-based approach. Then, since it is common practice in literature to express the member static loading as a fraction of its critical buckling value, the buckling behaviour of CHS columns is also addressed. Finally, the vibration behaviour of axially compressed CHS members (columns) is investigated, focusing mainly on the effect of the load magnitude on the fundamental frequency and vibration mode nature. Advantage is taken of the unique modal characteristics of GBT, (i) making it possible to perform accurate analyses involving only a few degrees of freedom and (ii) providing vibration mode representations expressed as linear combinations of deformation modes with clear structural meanings. For validation purposes, some GBT results are compared with numerical values obtained from shell finite element analyses carried out in the code ANSYS (SAS, 2009).

2 GBT FORMULATION

Because the cross-section displacement field is expressed as a linear combination of structurally meaningful deformation modes, GBT analyses involve solving equilibrium equation systems written in a very convenient modal form, thus leading to solutions that provide in-depth insight on the member structural response under consideration. The performance of a vibration analysis involves (i) a *cross-section analysis*, to obtain the deformation modes and corresponding mechanical properties, and (ii) the *member analysis*, *i.e.*, the solution of the vibration eigenvalue problem and the (modal) interpretation of the results determined (natural frequencies and vibration mode shapes).

Figure 1 depicts (i) a CHS prismatic member with radius r and wall thickness e, and (ii) the global coordinate system X, Y, Z. In order to account for the cross-section in-plane deformation, it is preferable to consider the local coordinate system x, θ, z, (a longitudinal coordinate $x \in [0; L]$, an angular coordinate $\theta \in [0; 2\pi]$ and a thickness coordinate $z \in [-e/2; +e/2]$ – u, v, w are the displacement components expressed in the local coordinate system.

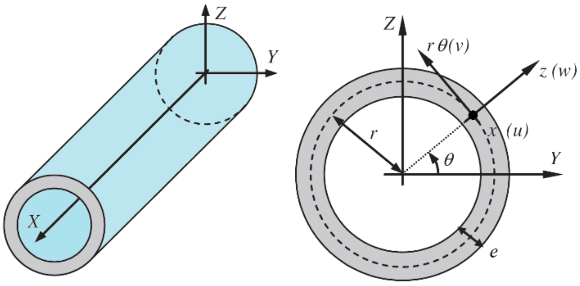

Figure 1. CHS member and global and local coordinate system and displacement components

According to the Love-Kirchoff assumptions, (i) the relations between the displacement components of an arbitrary point P (u^P, v^P, w^P), lying on a member wall, and the corresponding mid-plane ($z=0$) point P_0 (u, v, w) are expressed by

$$u^P = u - zw_{,x} \qquad v^P = \left(1+\frac{z}{r}\right)v - \frac{z}{r}w_{,\theta} \qquad w^P = w \tag{1}$$

and (ii) the relevant strain-displacement relations read (Sanders Jr., 1963), $(.)_{,x} \equiv d(.)/dx$,

$$\varepsilon_{xx} = u_{,x} + \frac{1}{2}w_{,x}^2 + \frac{1}{8}\left(v_{,x} - \frac{u_{,\theta}}{r}\right)^2 - zw_{,xx}$$

$$\varepsilon_{\theta\theta} = \frac{v_{,\theta}+w}{r} + \frac{1}{2}\left(\frac{v-w_{,\theta}}{r}\right)^2 + \frac{1}{8}\left(v_{,x} - \frac{u_{,\theta}}{r}\right)^2 - z\frac{w_{,\theta\theta}-v_{,\theta}}{r^2}$$

$$\gamma_{x\theta} = \frac{u_{,\theta}}{r} + v_{,x} + w_{,x}\left(\frac{w_{,\theta}-v}{r}\right) - z\left(\frac{4rw_{,x\theta}-3rv_{,x}+u_{,\theta}}{2r^2}\right) \quad . \tag{2}$$

In order to obtain a displacement representation compatible with the classical beam theory, each displacement component (u, v or w), at any given cross-section mid-surface point, must be expressed as a product of two *orthogonal* functions, (i) one depending on x (longitudinal coordinate) and t (time variable) and (ii) the other on θ (cross-section mid-line coordinate),

$$u(x,\theta,t) = u_k(\theta)\zeta_{k,x}(x,t) \qquad v(x,\theta,t) = v_k(\theta)\zeta_k(x,t) \qquad w(x,\theta,t) = w_k(\theta)\zeta_k(x,t) \quad , \tag{3}$$

where (i) the summation convention applies to subscript k, (ii) $u_k(\theta)$, $v_k(\theta)$ and $w_k(\theta)$ are functions characterising deformation mode k (Schardt, 1989 and Silvestre, 2007) and (iii) $\zeta_k(x,t)$ are functions describing the deformation mode amplitude variation both along the longitudinal direction and with time t.

The incorporation of (3) in (2) leads to the linear and non-linear (^{NL}) kinematical (strain-displacement) relations

$$\varepsilon_{xx} = u_k \zeta_{k,xx} - z w_k \zeta_{k,xx} \qquad \varepsilon_{\theta\theta} = \frac{v_{k,\theta} + w_k}{r}\zeta_k - z\frac{w_{k,\theta\theta} - v_{k,\theta}}{r^2}\zeta_k$$

$$\gamma_{x\theta} = \left(\frac{u_{k,\theta}}{r} + v_k\right)\zeta_{k,x} - z\left(\frac{4rw_{k,\theta} - 3rv_k + u_{k,\theta}}{2r^2}\right)\zeta_{k,x} \quad (4)$$

$$\varepsilon_{xx}^{NL} = \frac{1}{2} w_k w_i \zeta_{k,x}\zeta_{i,x} + \frac{1}{8}\left(v_k - \frac{u_{k,\theta}}{r}\right)\left(v_i - \frac{u_{i,\theta}}{r}\right)\zeta_{k,x}\zeta_{i,x} \quad . \quad (5)$$

Moreover, introducing (3) in (1) and differentiating the displacement components w.r.t. *t*, one obtains the velocity components

$$u_{,t}^P = (u_k - z\, w_k)\zeta_{k,xt} \qquad v_{,t}^P = \left(1 + \frac{z}{r}\right)v_k \zeta_{k,t} - \frac{z}{r} w_{,\theta}\zeta_{k,t} \qquad w_{,t}^P = w_k \zeta_{k,t} \quad . \quad (6)$$

Finally, since the thin-walled member is deemed made of an isotropic elastic material (*e.g.*, constructional steel), the constitutive relation reads

$$\begin{Bmatrix} \sigma_{xx} \\ \sigma_{\theta\theta} \\ \tau_{x\theta} \end{Bmatrix} = \begin{bmatrix} \frac{E}{1-\nu^2} & \frac{E\nu}{1-\nu^2} & 0 \\ \frac{E\nu}{1-\nu^2} & \frac{E}{1-\nu^2} & 0 \\ 0 & 0 & G \end{bmatrix} \begin{Bmatrix} \varepsilon_{xx} \\ \varepsilon_{\theta\theta} \\ \gamma_{x\theta} \end{Bmatrix} \quad , \quad (7)$$

where (i) E, G and ν are Young's modulus, shear modulus and Poisson's ratio, respectively, and (ii) σ_{ij} are the stress components.

2.1 Hamilton's Principle

The system of equilibrium equations describing the member dynamic or static behaviour must now to be established. Due to the complexity inherent to the problem under consideration, this task is performed using the Hamilton's principle, which may be expressed as

$$\int_{t_1}^{t_2} (\delta T - \delta V)dt = 0 \quad , \quad (8)$$

where (i) T and V are the member kinetic and potential energies and (ii) $[t_1, t_2]$ is an arbitrary time interval. Note that, in buckling analyses, because $\delta T=0$ and the internal energy variation δV is invariant with time, the equilibrium condition reduces to

$$\delta V = \delta U + \delta \Pi \quad , \quad (9)$$

where (i) δU is the member strain energy variation and (ii) $\delta\Pi$ is the potential of the applied (pre-buckling) stresses, which are given by

$$\delta U = \int_L (C_{ik}\zeta_{k,xx}\delta\zeta_{i,xx} + D_{ik}^1 \zeta_{k,x}\delta\zeta_{i,x} + D_{ik}^2 \zeta_k \delta\zeta_{i,xx} + D_{ki}^2 \zeta_{k,xx}\delta\zeta_i + B_{ik}\zeta_k \delta\zeta_i)dx$$

$$\delta\Pi = \int_L (\lambda W_j^0 X_{jik}\zeta_{k,x}\delta\zeta_{i,x})dx \qquad W_j^0 = C_{jj}\zeta_{j,xx}^0 \quad , \quad (10)$$

where (i) C_{ik} are stiffness components concerning *generalised* warping effects, (ii) D_{ik} are stiffness components dealing with *generalised* twisting, (iii) matrix $[B_{ik}]$ is related to the cross-section in-plane deformation (wall transverse bending) and (ii) X_{jik} are geometric stiffness components associated with the applied stress resultants W_j^0 – all components are defined in Silvestre (2007).

The variation of the member kinetic energy (virtual work of the inertia forces) involves terms related to the virtual work done by the translational (δT_T) and rotational (δT_R) inertia forces. Thus, one has

$$\delta T = \int_L \oint_e \int (\rho\, u^P_{,t} \delta\, u^P_{,t} + \rho\, v^P_{,t} \delta\, v^P_{,t} + \rho\, w^P_{,t} \delta\, w^P_{,t}) dzrd\theta dx = \delta T_T + \delta T_R \quad , \quad (11)$$

where (i) ρ is the material mass density and (ii) $u^P_{,t}, v^P_{,t}, w^P_{,t}$ are the velocity components at an arbitrary plate element point P. After incorporating (6) into (11) and integrating over the whole cross-section (coordinates θ and z), one obtains expressions for the two δT terms as

$$\delta T_T = \int_L \oint_e \int \rho \left(u_{,t}\delta u_{,t} + v_{,t}\delta v_{,t} + \frac{z^2}{r^2} v_{,t}\delta v_{,t} + w_{,t}\delta w_{,t} \right) dzrd\theta dx \quad (12)$$

$$\delta T_R = \int_L \oint_e \int \rho \left(z^2 w_{,xt}\delta w_{,xt} - \frac{z^2}{r^2} v_{,t}\delta w_{,\theta t} - \frac{z^2}{r^2} w_{,\theta t}\delta v_{,t} + \frac{z^2}{r^2} w_{,\theta t}\delta w_{,\theta t} \right) dzrd\theta dx \quad . \quad (13)$$

Inserting (3) into (12)-(13) and integrating over the cross-section, one gets

$$\delta T_T = \int_L (Q^I_{ik}\zeta_{k,xt}\delta\zeta_{i,xt} + R^I_{ik}\zeta_{k,t}\delta\zeta_{i,t}) dx \quad (14)$$

$$\delta T_R = \int_L (Q^{II}_{ik}\zeta_{k,xt}\delta\zeta_{i,xt} + R^{II}_{ik}\zeta_{k,t}\delta\zeta_{i,t}) dx \quad , \quad (15)$$

where tensors Q^I (out-of-plane translational inertia), Q^{II} (out-of-plane rotational inertia), R^I (in-plane translational inertia) and R^{II} (in-plane rotational inertia) are the GBT inertia matrices – for members with uniform mass density and thickness, these matrices read

$$Q^I_{ik} = \rho e \oint (u_i u_k) rd\theta \qquad Q^{II}_{ik} = \frac{\rho e^3}{12} \oint (w_i w_k) rd\theta \quad (16)$$

$$R^I_{ik} = \rho \oint \left(e v_i v_k + \frac{e^3}{12r^2} v_i v_k + e w_i w_k \right) rd\theta \qquad R^{II}_{ik} = \frac{\rho e^3}{12r^2} \oint (w_{i,\theta} w_{k,\theta} - w_{i,\theta} v_k - v_i w_{k,\theta}) rd\theta \quad . \quad (17)$$

Finally, defining matrices Q_{ik} (out-of-plane inertia) and R_{ik} (in-plane inertia) as

$$Q_{ik} = Q^I_{ik} + Q^{II}_{ik} \qquad R_{ik} = R^I_{ik} + R^{II}_{ik} \quad (18)$$

and introducing these expressions into (14) and (15), one is led to

$$\delta T = \int_L (Q_{ik}\zeta_{k,xt}\delta\zeta_{i,xt} + R_{ik}\zeta_{k,t}\delta\zeta_{i,t}) dx \quad . \quad (19)$$

2.2 Cross-Section Analysis

The cross-section analysis comprises a set of rather complex sequential operations, already described in detail by Schardt (1989) and Silvestre (2007). Nevertheless, it is worth drawing the reader's attention to the following aspects, concerning the concepts and procedures involved:

(i) The deformation modes consist of a "*shell-type*" mode family (modes originally considered by Schardt, 1989), an *axis-symmetric* mode, a *torsion* mode (both first introduced by Silvestre, 2007) and (warping) *shear modes* (first introduced in Basaglia *et al*., 2015).

(ii) Like the conventional deformation modes of unbranched open cross-sections (*e.g.*, Bebiano *et al.*, 2015), the "*shell-type*" modes, based on the assumption of null membrane shear strains and transverse extensions, constitute the core of the GBT analysis of CHS members and structural systems – Figure 2 shows the in-plane deformed configurations of the first *14* shell-type modes.

(iii) The *axisymmetric* mode (identified by subscript **a**) involves only in-plane displacements and accounts for the cross-section deformation due to the extension in the circumferential direction – thus, the corresponding displacement profile exhibits $u_a=0$, $v_a=0$ and $w_a=1$ (see Fig. 3).

(iv) The *torsion* mode (identified by subscript **t**) has a displacement profile characterised by $u_a=0$, $v_a=r$ and $w_a=0$ (see Fig. 3).

(v) The *shear* modes (identified by subscript **s**) involve exclusively warping displacements – the displacement profiles of mode k are defined by different expressions for even and odd k values – Figure 4 shows the warping displacements of the 8 shear modes considered (k=**1s**,…,**8s**).

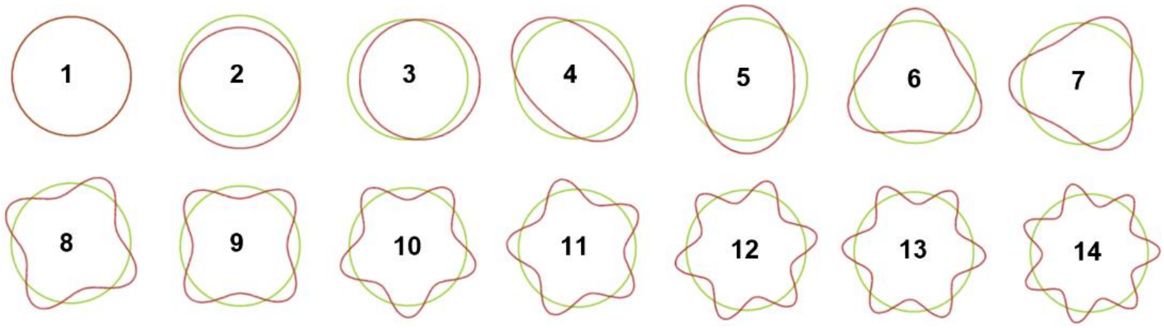

Figure 2. First *14* shell-type deformation modes for circular hollow cross-sections

Figure 3. Axis-symmetric (a) and torsion (t) deformation modes

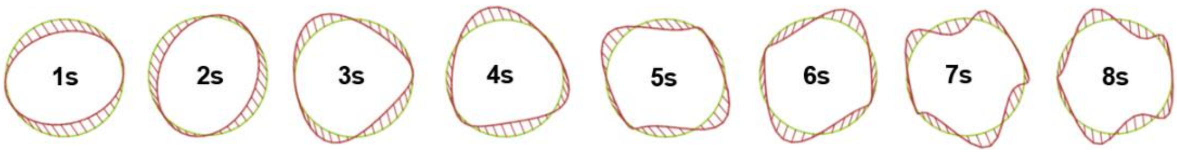

Figure 4. Warping displacement profiles associated with the first *8* shear modes

2.3 Member Analysis

After determining the deformation modes, the equilibrium equation system defining the dynamic problem can be readily established as

$$C_{ik}\zeta_{k,xxxx} - D_{ik}\zeta_{k,xx} + B_{ik}\zeta_k - Q_{ik}\zeta_{k,xxtt} + R_{ik}\zeta_{k,tt} - X_{jik}\left(W_j^0\zeta_{k,x}\right)_{,x} = 0 \quad . \quad (20)$$

For members moving in synchronous configurations, the amplitude functions ζ_k can be written as

$$\zeta_k(x,t) = \phi_k(x)Y(t) \quad , \quad (21)$$

where $\phi_k(x)$ is a longitudinal shape function and $Y(t)$ is a time-dependent function satisfying the free vibration harmonic equation of motion $Y_{,tt}+\omega^2 Y=0$ (ω is the angular frequency of vibration) –

thus, they may be expressed as

$$\zeta_{k,tt} = -\omega^2 \zeta_k \quad . \quad (22)$$

It is worth noting that, in the context of geometrically linear static analyses, one has

$$Y(t) = 1 \quad \Leftrightarrow \quad \zeta_k = \phi_k \quad . \quad (23)$$

The insertion of (18) into (16) leads to the final system of equilibrium equations,

$$C_{ik}\phi_{k,xxxx} - D_{ik}\phi_{k,xx} + B_{ik}\phi_k - \omega^2\left(R_{ik}\phi_k - Q_{ik}\phi_{k,xx}\right) - X_{jik}\left(W_j^0 \phi_{k,x}\right)_{,x} = 0 \quad , \quad (24)$$

which depends exclusively on derivatives with respect to the longitudinal coordinate *x*.

The methods that have been employed to solve the above GBT eigenvalue problems are fairly standard in structural analysis. They include (i) Galerkin's method, used by Silvestre (2007) to perform the CHS member buckling analyses, and (ii) the finite element method, based on a beam element formulation specifically developed for to GBT analyses and employed so far to analyse members with flat-walled (open and/or closed) cross-sections (*e.g.*, Bebiano *et al.*, 2015). At this point, it is worth mentioning that the GBT results presented in this work were obtained by means of a beam finite element specifically developed for CHS members – the main steps and procedures involved in the formulation of this finite element are briefly described next (Basaglia *et al.*, 2015):

(i) Approximate the modal amplitude functions $\phi_k(x)$ by means of linear combinations of (i_1) Lagrange cubic polynomial primitives, for the axial extension and warping shear deformation modes (those involving solely warping displacements *u*) and (i_2) Hermite cubic polynomials, for the remaining shell-type, axis-symmetric and torsion deformation modes. Then, one has

$$\phi_k(x) = \Psi_\alpha(\xi) d_{k\alpha}^{e.i} = \Psi_1 d_{k1}^{e.i} + \Psi_2 d_{k2}^{e.i} + \Psi_3 d_{k3}^{e.i} + \Psi_4 d_{k4}^{e.i} \quad , \quad (25)$$

where (i_1) Ψ_α are either Lagrange cubic polynomial primitives or Hermite polynomials and (i_2) $d_{k\alpha}^{e.i}$ are the generalised displacements of finite element *i*.

(ii) The various sub-matrix components of the finite element linear stiffness $[K_e]$, geometric stiffness $[G_e]$ and mass $[M_e]$ matrices are determined by means of the expressions

$$K_{ik\alpha\beta}^{(e)} = C_{ik}\int_{L_e} \Psi_{\alpha,xx}\Psi_{\beta,xx}\,dx + B_{ik}\int_{L_e}\Psi_\alpha\Psi_\beta\,dx + D_{ik}^1\int_{L_e}\Psi_{\alpha,x}\Psi_{\beta,x}\,dx + $$
$$+ D_{ik}^2\int_{L_e}\Psi_{\alpha,xx}\Psi_\beta\,dx + D_{ki}^2\int_{L_e}\Psi_\alpha\Psi_{\beta,xx}\,dx \quad (26)$$

$$G_{ik\alpha\beta}^{(e)} = W_j^0 X_{jik}\int_{L_e}\Psi_{\alpha,x}\Psi_{\beta,x}\,dx \qquad M_{ik\alpha\beta}^{(e)} = Q_{ik}\int_{L_e}\Psi_{\alpha,x}\Psi_{\beta,x}\,dx + R_{ik}\int_{L_e}\Psi_\alpha\Psi_\beta\,dx \quad , \quad (27)$$

where the roman (*i*, *j*, *k*) and greek (α, β) subscripts identify the *deformation mode* and *degree of freedom* (modal generalised displacement), respectively.

(iii) Taking into account the member *support conditions*, expressed in terms of modal d.o.f. (usually modal amplitude values and/or derivatives at the member end cross-sections – see (25)), perform the assembly procedure leading to the discrete vibration eigenvalue problem

$$([K] - [G] - \omega^2[M])\{d\} = \{0\} \quad , \quad (28)$$

where (iii_1) $[K]$ and $[G]$ are the member linear and geometrical stiffness matrices, (iii_2) $[M]$ is the member mass matrix and (iii_3) $\{d\}$ is the generalised modal amplitude vector – its components are the (unknown) values and/or derivatives of the GBT deformation mode amplitudes at the member nodes (finite element end cross-sections).

3 ILLUSTRATIVE EXAMPLES

In order to validate and illustrate the application and potential of the proposed GBT-based beam finite element approach, numerical results are presented and discussed next. They concern fixed-ended CHS steel ($E=210GPa$, $v=0.3$ and ρ=7.85g/cm^3) members with radius $r=60mm$ and wall thickness $t=1.2mm$. The variation of the lower natural frequencies and vibration mode shapes with the member length is investigated. After analysing the (i) vibration behaviour of load-free members and (ii) the buckling behaviour uniformly compressed columns, the vibration behaviour of axially compressed members is finally addressed – the static applied uniform compression (P) is always expressed as a percentage of the corresponding critical buckling value (P_{cr}). For validation purposes, most GBT results are compared with values yielded by ANSYS (SAS, 2009) shell finite element analyses.

3.1 Load-Free Member Vibration

The curves depicted in Figure 5 provide the variation of the first three natural frequencies (ω_f, ω_2 and ω_3 – subscript f stands for “fundamental”) with the length L, as well as the corresponding vibration mode longitudinal half-wave numbers (n_s) – note that there is always a set of two vibration modes corresponding to the same frequency value (multiplicity 2 eigenvalues), which implies the existence of a vibration mode subspace. In order to enable a clearer visualisation of the curves in Figure 5, different vertical scales are adopted for $10<L<100cm$ and $100<L<1000cm$. The ANSYS values, providing validation for the GBT results, are identified by white circles (ω_f), squares (ω_2) and values, providing validation for the GBT results, are identified by white circles (ω_f), squares (ω_2) and triangles (ω_3). Figure 6 concerns members with $L=10$, 60, 300 and $500cm$, and shows (i) ANSYS 3D vibration mode shapes and (ii) the GBT deformation modes participating in the vibration modes. The comparison between the GBT and ANSYS vibration results prompts the following remarks:

(i) The GBT and ANSYS frequency values agree perfectly, as the differences never exceed *2.5%*. Moreover, there is also very close agreement between the vibration mode shapes provided by the two analyses, as can be readily seen by looking at Figures 2 to 4 and 6.

(ii) The three first natural frequencies decrease monotonically with L and tend to zero as L goes to infinity. While ω_f and ω_2 are very close for $L\approx25$, 55 and $180cm$, the ω_2 and ω_3 values are virtually identical for $L\approx20$, 40, 100 and $300cm$.

(iii) The fundamental vibration modes always exhibit a single half-wave, regardless of the member length. On the other hand, the second and third vibration modes may have more than one half-wave, depending on the member length.

(iv) Unlike the column buckling modes, the member vibration modes always have a contribution from *shear modes* (*i.e.*, modes involving non-linear warping displacements), as was already noted by Bebiano (2010), in the context of the vibration of open cross-section members.

(v) For $L<50cm$, the fundamental vibration occurs in a *shell-type* GBT deformation mode of an order higher than that corresponding to the second vibration mode – *e.g.*, for $L=10cm$ the fundamental and second vibration modes have contributions from modes **10** and **8**, respectively. However, note that the contribution of the *shear modes* increases with the vibration mode order.

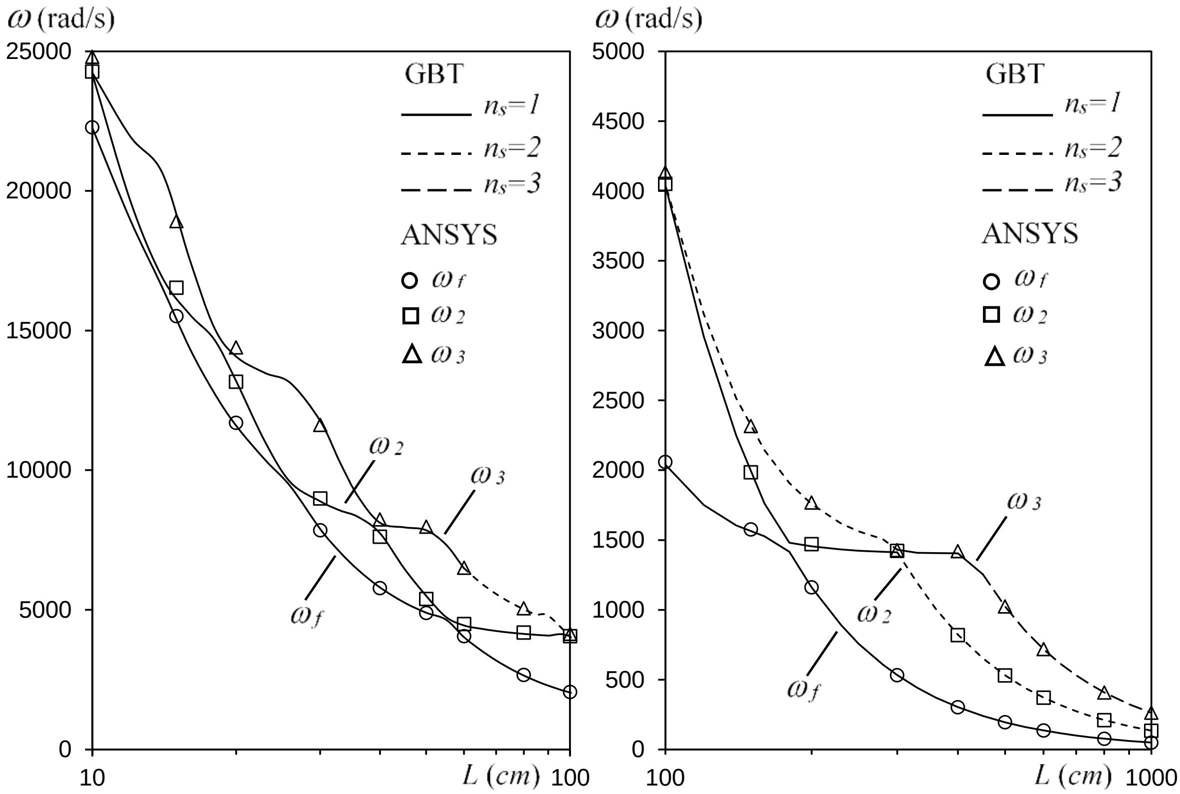

Figure 5. Frequency curves $\omega_f(L)$, $\omega_2(L)$ and $\omega_3(L)$

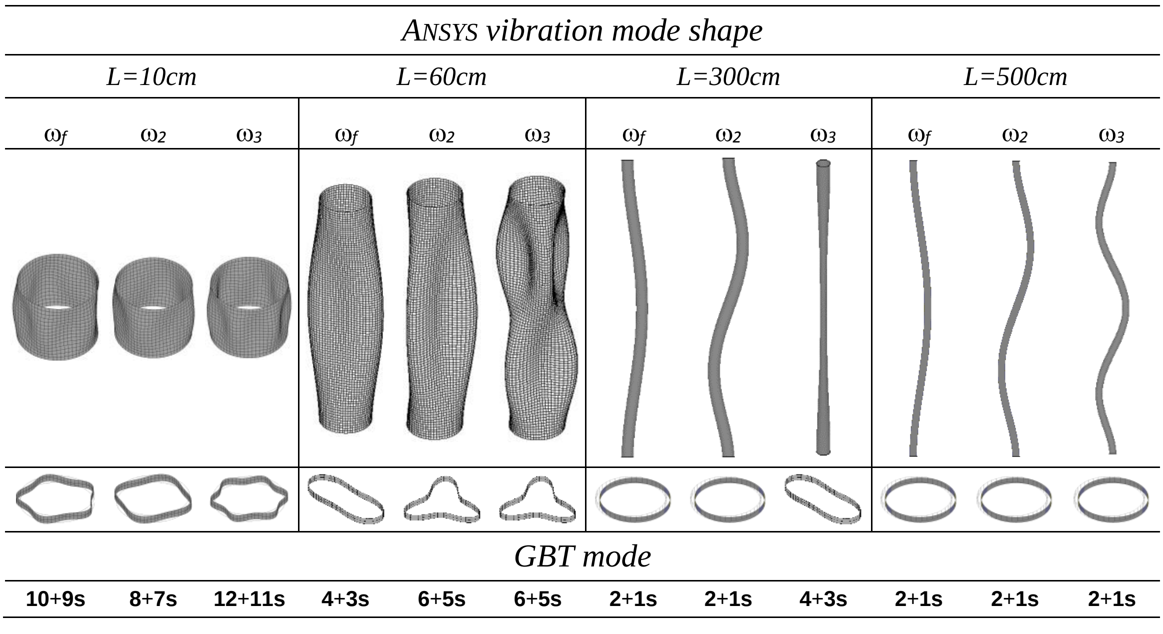

Figure 6. ANSYS vibration mode shapes yielded and GBT modes participating in the vibration mode

3.2 Fixed-Ended Column Buckling

Figure 7 shows GBT-based buckling results, namely the variation of the fixed-ended column critical buckling load P_{cr} (kN) and mode shape with the length L (cm). For several L values, ANSYS shell finite element results are also displayed. The following conclusions can be drawn from the observation of these column buckling results:

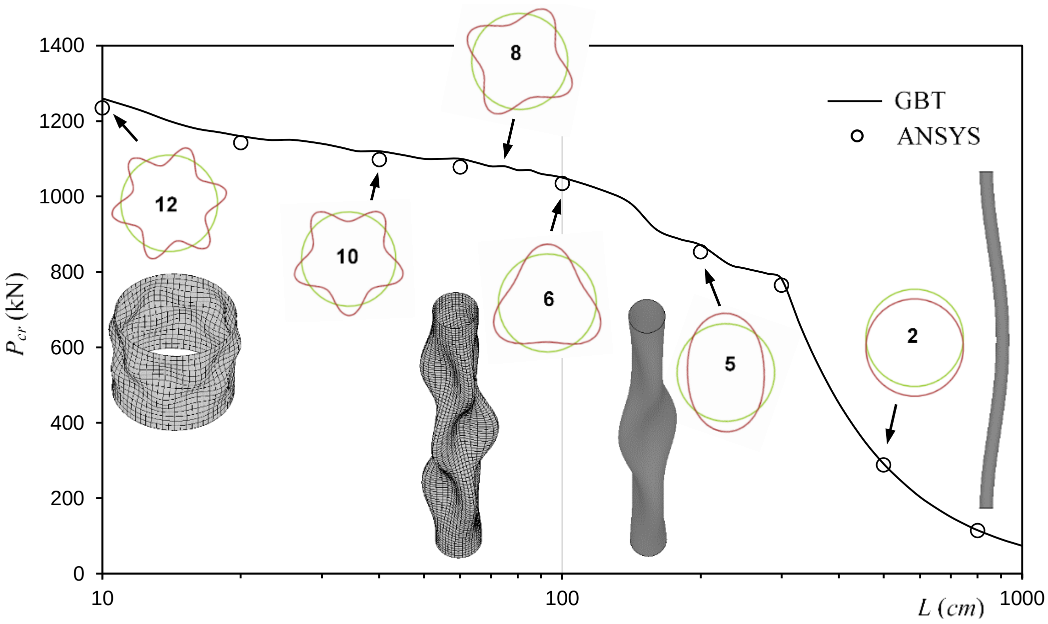

Figure 7. Variation of the critical buckling load (P_{cr}) and mode shape with the column length (L)

(i) The GBT and ANSYS critical buckling loads are extremely close – differences below *3%*. In addition, there is an excellent agreement between the GBT and ANSYS buckling mode shapes.

(ii) The buckling load P_{cr} always decreases with L – however, for $L>300$ *cm*, this P_{cr} decrease takes place at a much higher rate.

(iii) For $L\leq 60$ *cm*, the column buckles in critical shell-type modes with *5* and *6* circumferential half-waves (modes **12** and **10**) and *2* to *7* longitudinal half-waves. For $60<L\leq 120$ *cm*, buckling occurs in a critical shell-type mode with *3* and *4* circumferential half-waves (modes **6** and **8**) and *3* to *6* longitudinal half-wave. For $120<L\leq 300$ *cm*, the column buckles in shell-type mode **2** with *2* to *4* longitudinal half-waves. For $L>300$ *cm*, the column buckles in single half-wave flexural mode.

3.3 Axially-Compressed Member (Column) Vibration

Finally, the vibration of uniformly axially compressed members (columns) is investigated – the axial compression level is defined by the parameter $P^0 \equiv W_1^0$, taken as fraction (α) of the critical buckling value (*i.e.*, $P^0 \equiv \alpha P_{cr}$). Figure 8 makes it possible to assess the influence of the axial compression on the member fundamental frequency ω_f. Moreover, the 3D views of the buckling and vibration modes yielded by the ANSYS analyses, presented in Figure 9 for $L=40cm$ and $\alpha=0,\ 0.6,\ 0.95,\ 0.99$, provide information on the evolution of the fundamental vibration mode nature as the axial compression level increases. The results presented in these two figures prompt the following remarks:

(i) The presence of axial compression only causes a visible fundamental frequency drop (*i.e.*, more than *5%*) for $\alpha>0.1$ – a substantial fundamental frequency drop (*i.e.*, more than *30%*) occurs for $\alpha>0.6$. In order to confirm these particular findings, the corresponding ANSYS values were determined and are also shown in Figure 8 – an excellent agreement can be observed, both in terms of the frequency values and vibration mode shapes (not shown here).

(ii) The comparison between the modal amplitude functions for $\alpha=0$ e $\alpha\neq 0$ shows that the fundamental vibration modes of the load-free member and the axially compressed member with $\alpha<0.95$ are very similar. On the other hand, for α close to 1.0 the vibration mode changes quite drastically and practically replicates the column critical buckling mode – indeed, for α=0.99 the fundamental vibration and buckling modes virtually coincide, as clearly shown in Figure 9.

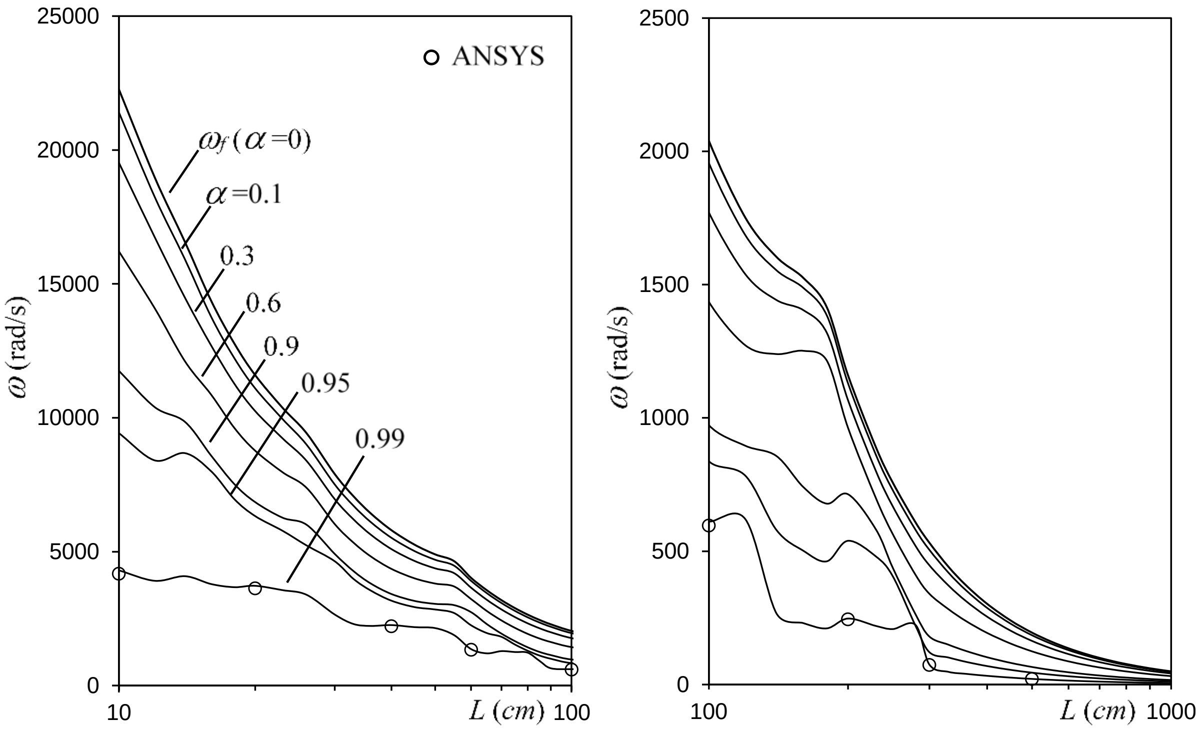

Figure 8. Variation of the fundamental frequency ω_α with the member length and axial compression level

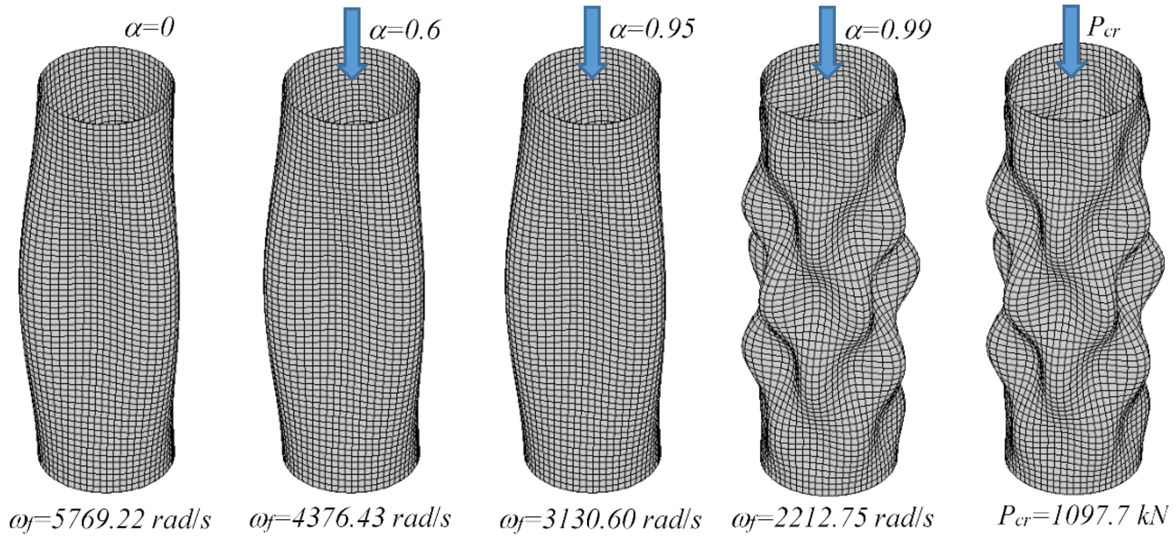

Figure 9. CHS member with *L=40cm*: fundamental vibration modes for α=*0, 0.6, 0.95, 0.99* and critical buckling mode

4 CONCLUSION

The paper reported the results of an investigation on the use of a GBT-based beam finite element approach to analyse the vibration and buckling behaviours of CHS members. After a very brief review of the most relevant concepts involved in performing a GBT analysis, the paper described the procedures required to obtain the member overall linear and geometric stiffness matrices, as well as the mass matrix. Finally, the application and capabilities of the developed GBT-based beam finite element approach were illustrated by means of the presentation and discussion of numerical results concerning the vibration behaviour of load-free and axially compressed cold-formed steel CHS members. The study focused on the influence of the axial compression level on the natural frequencies and vibration mode shapes − in particular, it was numerically confirmed that the fundamental vibration mode shape tends to the column critical buckling mode shape as the axial compression level approaches P_{cr}. For validation purposes, most of the GBT results were compared with values obtained by means of ANSYS shell finite element analyses – an excellent agreement was observed in all cases, for both the natural frequency values and the vibration mode shapes.

ACKNOWLEDGEMENTS

The first author gratefully acknowledges the financial support provided by the *Conselho Nacional de Desenvolvimento Científico e Tecnológico* (CNPq – Ministry of Science, Technology and Innovation of Brazil), through project nº 446679/2014-3.

REFERENCES

Basaglia, C., Camotim, D. & Silvestre, N., 2015. Buckling and vibration analysis of cold-formed steel CHS members and frames using Generalized Beam Theory. *International Journal of Structural Stability and Dynamics*, vol. 15, n. 8, pp. 1540021-1 – 1540021-25.

Bebiano, R., 2010. *Stability and Dynamics of Thin-Walled Members: Application of Generalised Beam Theory*. Ph.D. Thesis in Civil Engineering, IST, Technical University of Lisbon, Portugal.

Bebiano, R., Gonçalves, R., Camotim, D., 2015. A cross-section analysis procedure to rationalise and automate the performance of GBT-based structural analyses. *Thin-Walled Structures*, vol. 92, pp. 29-47.

Camotim, D., Basaglia, C., Bebiano, R., Gonçalves, R. & Silvestre, N., 2010. Latest developments in the GBT analysis of thin-walled steel structures. *Proceedings of International Colloquium on Stability and Ductility of Steel Structures* (SDSS'Rio 2010). E. Batista *et. al.*, eds., Federal University of Rio de Janeiro, Rio de Janeiro, vol. 1, pp. 33-58.

Gardner, L. & Nethercot, D.A., 2004. Numerical modeling of stainless steel structural components – a consistent approach. *Journal of Structural Engineering* (*ASCE*), vol. 130, n. 10, pp. 1586-1601.

Sanders Jr., J.L., 1963. Non-linear theories for thin shells. *Quarterly of Applied Mathematics*, vol. 21, n. 1, pp. 21-36.

Schardt, R., 1989. *Verallgemeinerte Technishe Biegetheorie*. Springer-Verlag, Berlin, (1989) (German).

Silvestre, N., 2007. Generalised beam theory to analyse the buckling behaviour of circular cylindrical shells and tubes. *Thin-Walled Structures*, vol. 45, n. 2, pp. 185-198.

Swanson Analysis Systems (SAS), 2009. Inc.: ANSYS reference manual, version 12.

Teng, J.G., 1996. Buckling of thin shells: recent advances and trends. *Applied Mechanics Reviews* (*ASME*), vol. 49, n. 4, pp. 263-274.